The Hysteretic Behavior of Partially Pre-Stressed Beam-Column Joint Sub-assemblages Made of Reactive Powder Concrete

Siti Aisyah Nurjannah[1,*], Bambang Budiono[2], Iswandi Imran[2] & Saptahari Sugiri[2]

[1]Post-Graduate Program of Civil Engineering Department,
Faculty of Civil and Environmental Engineering, Institut Teknologi Bandung,
Jalan Ganesha No. 10, Bandung 40132, Indonesia
[2]Structure Research Group, Civil Engineering Department,
Faculty of Civil and Environmental Engineering, Institut Teknologi Bandung,
Jalan Ganesha No. 10, Bandung 40132, Indonesia
*E-mail: sanurjannah@gmail.com

Abstract. Reactive powder concrete (RPC) is an alternative to normal concrete (NC) allowing for significantly higher strength of partially pre-stressed concrete structures. In the Indonesian national standard SNI 03-2847-2013 (2013) and the American standard ACI 318-14 (2014), the partial pre-stressed ratio (PPR) is limited to a maximum of 25.0 percent to ensure that pre-stressed concrete structures remain ductile and capable to dissipate seismic energy sufficiently. The objective of this experimental study was to investigate the hysteretic performance of partially pre-stressed-RPC (PP-RPC) for both interior and exterior beam-column joint sub-assemblages. Four specimens with different levels of PPR were tested with a combination of constant axial compression and cyclic lateral loads. The PPR used for the first and the second two specimens were 22.8% and 33.8%, respectively. The strength of the RPC was 101.60 MPa for all specimens. The results showed that increasing the PPR of PP-RPC improves its hysteretic performance. The best performing specimen, with a PPR of 33.8%, had a ductility that was 1.97 times that of the specimen with a PPR of 22.8%.

Keywords: *displacement ductility; energy dissipation; partial pre-stressed ratio; reactive powder concrete; seismic performance level.*

1 Introduction

Ductility and energy dissipation are vital properties of reinforced concrete structures. They are ensured by limiting the partial pre-stressed ratio (PPR) to a maximum of 25.0% [1,2]. Reactive powder concrete (RPC) is used to improve the ratio between the strength and the dimensions of a structure due to its higher performance in terms of compressive strength, tensile strength, ductility, and durability than normal concrete (NC) [3,4]. The first developed RPC had a compressive strength of 170-230 MPa, flexural strength of 25-60 MPa, and

Received March 28th, 2016, Revised September 5th, 2016, Accepted for publication October 31st, 2016.
 ISSN: 2337-5779, DOI: 10.5614/j.eng.technol.sci.2016.48.5.4

elastic modulus of 54-60 GPa [3]. RPCs do not contain coarse aggregates to increase the interlocking force between their constituents; an additional material can be used for this purpose. One example of such a material is polypropylene micro fibers. These fibers serve as bridges to connect concrete sections divided by micro cracks and especially to prevent autogenous shrinkage at an early age, as well as to reduce brittleness and increase ductility [5]. In this study, the RPC materials were composed of cement, silica fume, silica sand, silica flour, polypropylene micro fibers, super-plasticizer, and water.

The research objective was to investigate the hysteretic performance of partially pre-stressed-RPC (PP-RPC) for interior and exterior beam-column joint sub-assemblages with different levels of PPR.

2 Experimental Method

In this experiment, interior and exterior beam-column joint sub-assemblage (BCS-I and BCS-E, respectively) specimens made from PP-RPC were given constant axial and cyclic lateral loads in order to analyze their performance. The analysis of the performance included strength, relative energy dissipation ratio, hysteretic curve gradient of load-deflection [6], ductility, energy dissipation, and seismic performance level [7]. Based on previous research reports [8,9], each specimen of both BCS-I and BCS-E was reinforced by partial pre-stressing with a PPR value of 33.8% and 22.8% to determine the effect of PPR levels on specimen performance. The RPC aggregates were obtained from local distributors, while the polypropylene fibers were imported.

2.1 Material Properties of Specimens

Research on RPC materials was first conducted by Richard and Cheyrezy [3,4] and developed by Gowripalan using a different composition [10]. Menefy studied RPC bending loads using the composition described by Gowripalan and produced RPC cylinders with compressive strengths that ranged between 125 and 154 MPa [11]. In his experiment, the RPC beams exhibited superior performance compared to NC beams. In the present research, the RPC material composition per 1 m^3 was based on [12] with increased polypropylene fibers at 0.08% volume fraction to improve ductility and tensile strength (Table 1).

Table 1 Mixture composition of RPC for 1 m3.

Material	Material Weight (%)	Material	Material Weight (%)
Portland cement	39.09	Silica flour	2.72
Silica fume	4.69	Water	8.58
Super-plasticizer	1.11	Polypropylene fiber	0.03 (0.08% volume fraction)
Silica sand	43.78		

Silica sand and silica flour maximum diameters were 600 μm and 0.05 μm, respectively. Polypropylene fiber diameter and length were 18 micron and 12 mm, respectively.

2.2 Design of the Specimens

Two BCS-I and two BCS-E specimens were reinforced at PPR values of 33.8% and 22.8% (Table 2).

Table 2 Four specimens in the experimental tests.

Specimen	Type	Transversal Reinforcement Space of Beam Plastic Hinges *s* (mm)	PPR (%)
BCS-I-1B-33.8	Interior	50	33.8
BCS-E-1A-33.8	Exterior	100	33.8
BCS-I-2B-22.8	Interior	50	22.8
BCS-E-2B-22.8	Exterior	50	22.8

Each specimen had the same dimensions in terms of beams and columns. The reinforcement details of each specimen are shown in Figures 1 to 4. The strands in the BCS were pre-stressed at 78% of ultimate stress prior to concrete casting and were placed un-bonded in the plastic hinges [1, 2].

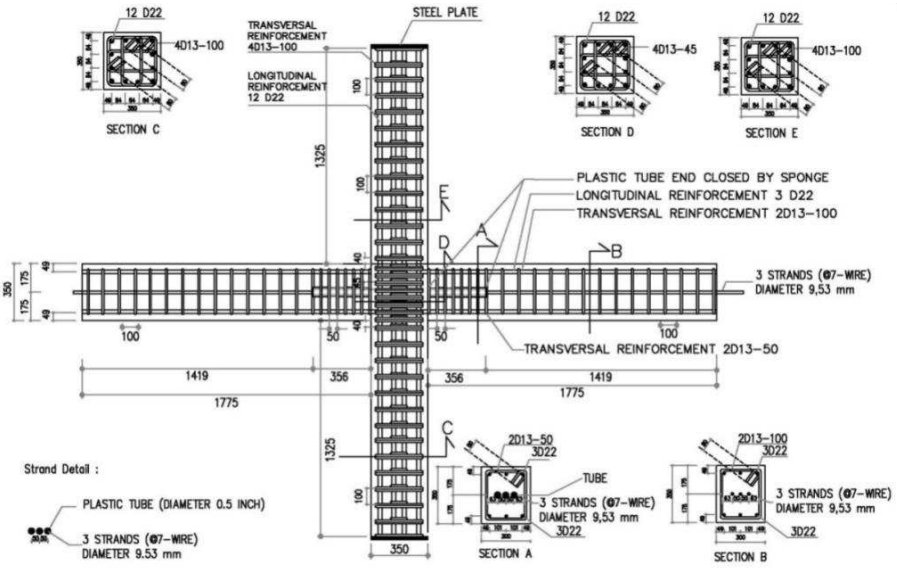

Figure 1 Specimen BCS-I-1B-33.8.

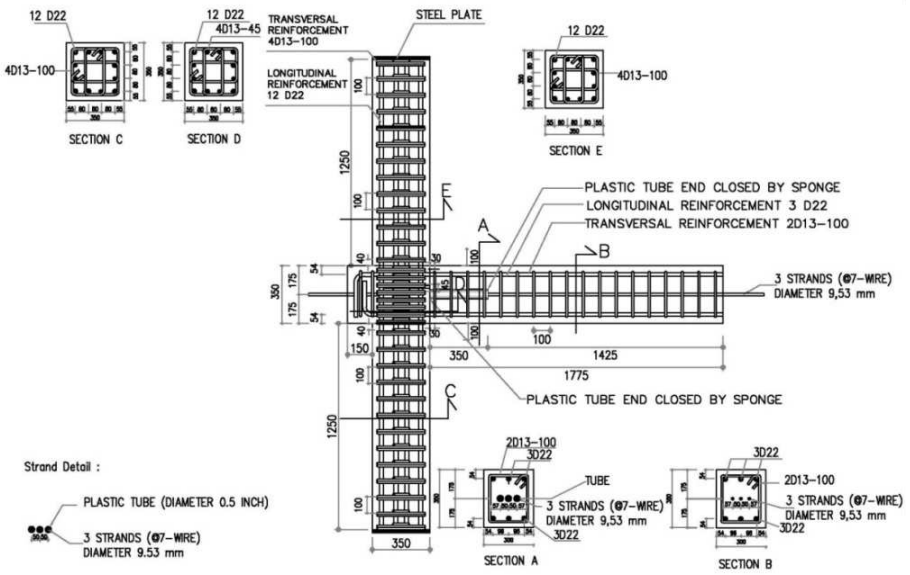

Figure 2 Specimen BCS-E-1A-33.8.

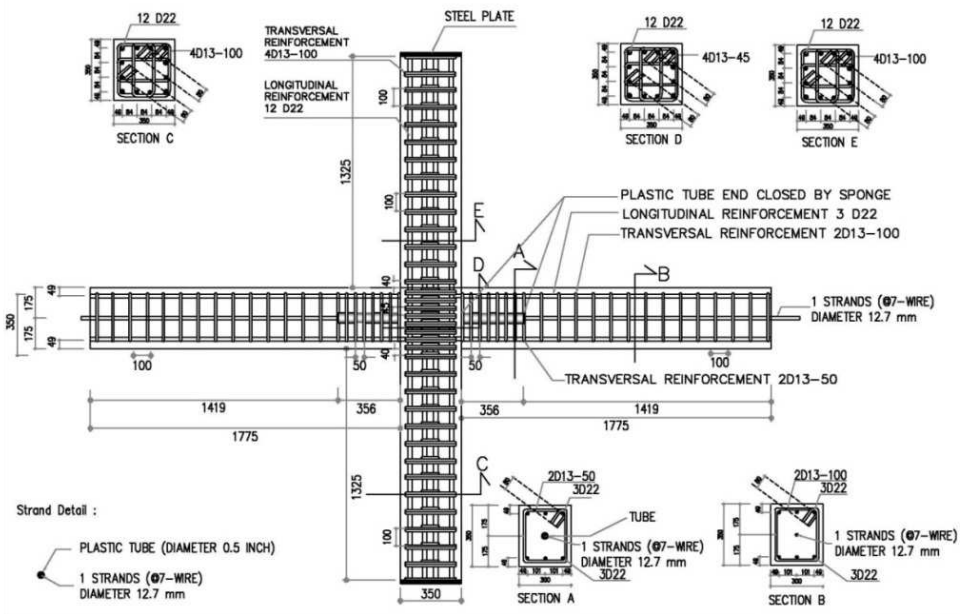

Figure 3 Specimen BCS-I-2B-22.8.

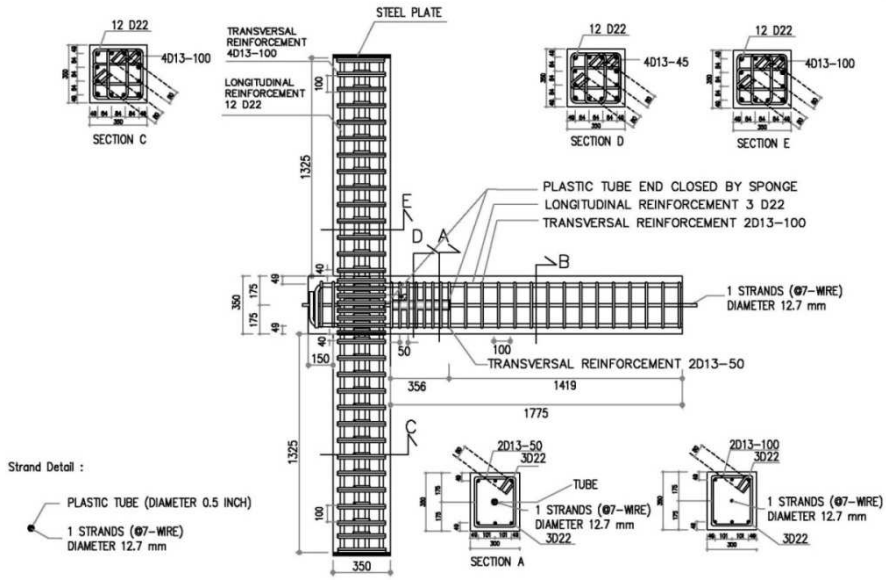

Figure 4 Specimen BCS-E-2B-22.8.

2.3 Instrumentation

The instruments used in the experiment were linear variable displacement transducers (LVDTs) for measuring displacement and strain gauges for measuring the strain on the mild steel bars and pre-stressed strands. The data from the instruments were transferred to a data logger, recorded by a computer, and displayed on a computer screen. The LVDTs were placed in locations where the specimens were expected to develop extreme displacement and in restraints where they would not be displaced by large amounts.

2.4 Loading System

In the experiment, each specimen was given a constant axial compressive force on the top of the column of $0.1f_c'A_g$ (f_c' is the characteristic compressive strength of concrete; A_g is the area of the column), and was also given displacement control cyclic lateral loads [6]. The cyclic lateral loading history is shown in Figure 5.

Initially, the drift ratio was set to 0.2% for three cycles. It was then increased to 5.00% at the end of the loading process. Among the drift ratio increments, there were small cycles that served to relax the specimens prior to the next increased lateral load.

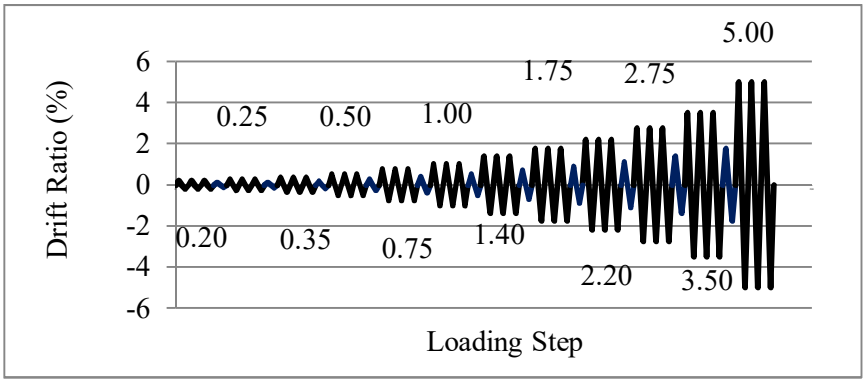

Figure 5 Lateral loading history (deflection control).

2.5 Test Setup

All specimens were used as models for a typical structure system, with the ends of the beams as roller restraints, the bottom of the columns as pin restraints, and the top of the columns able to move laterally, as shown in Figure 6. The tests were conducted in the Laboratory of Structure and Building Construction, Center of Research and Development for Human Settlements, Ministry of Public Works.

(a) Interior beam-column joint sub-assemblage specimen.

(b) Exterior beam-column joint sub-assemblage specimen.

Figure 6 Test setup.

3 Experimental Results and Discussion

3.1 Material Properties

Thirty-four 100/200 RPC cylinders with an age of 28 days were tested. The cylinders exhibited a range of compressive strengths between 100.33 and 143.77 MPa, with an average of 117.13 MPa, standard deviation of 11.45 MPa, and characteristic compressive strength of 101.79 MPa. Normally, RPC has a higher compressive strength than that reported in the present study. The lower compressive strength was influenced by the characteristic of the aggregates.

Fourteen other 100/200 RPC cylinders were also tested on the same day as the BCS specimens. The results showed compressive strengths ranging from 100.69 and 135.91 MPa, with an average of 116.71 MPa, standard deviation of 11.27 MPa, and characteristic compressive strength of 101.60 MPa (Table 3).

Table 3 Material properties of RPC.

No.	Age	Compressive Strength	No.	Age	Compressive Strength
	t	f_c		t	f_c
	(Days)	(MPa)		(Days)	(MPa)
1	35	127.88	8	42	103.42
2	35	113.16	9	42	125.65
3	35	105.06	10	42	135.91
4	35	117.70	11	42	119.66
5	35	105.65	12	42	124.75
6	35	100.69	13	42	121.74
7	42	104.58	14	56	128.01

Three 100/200 RPC cylinders were tested and each cylinder was equipped with two vertical and two horizontal concrete strain gauges (PL-60-11), which were installed in a Wheatstone full bridge configuration to measure strain. The stress-strain curves are shown in Figure 7. The ultimate strain ranged from 0.92% to 1.24% and the compressive strength ranged from 109.57 to 143.77 MPa.

In addition to the RPC material, D22 and D13 mild steel bars were used for longitudinal and transversal reinforcement respectively, while D9.5 and D12.7 7-wire uncoated low relaxation strands were used as pre-stressed strands. The results of the tensile strength tests performed on the steel bars and strands (Tables 4 and 5) satisfied the criteria [13].

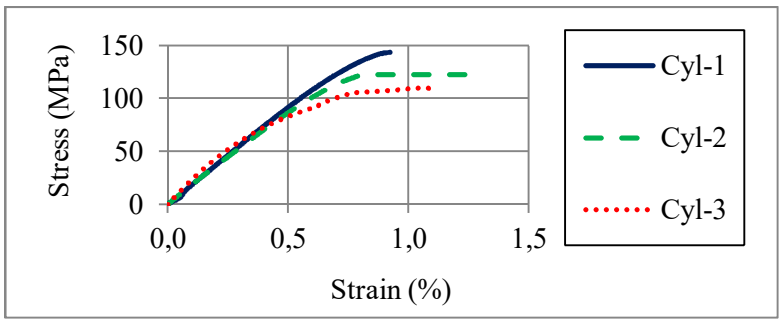

Figure 7 Stress-strain curves of reactive powder concrete.

Table 4 Material properties of mild steel bars.

Diameter	Length	Mass	Yield Stress	Ultimate Stress
D **(mm)**	***L*** **(mm)**	***m*** **(kg/m)**	f_y **(MPa)**	f_u **(Mpa)**
13	993	0.997	425.45	593.99
13	998	0.992	424.38	595.89
13	985	0.995	398.12	585.14
22	1007	2.979	450.76	601.11
22	1005	2.985	492.00	654.29

Table 5 Material properties of strands.

Diameter	Yield Load	Ultimate Load	Yield Stress	Ultimate Stress
D **(mm)**	F_{py} **(kN)**	F_{pu} **(kN)**	f_{py} **(Mpa)**	f_{pu} **(Mpa)**
9.5	109.42	109.53	1988.41	1990.33
9.5	107.85	110.55	1959.88	2008.84
9.5	107.65	112.55	1956.23	2045.26
12.7	99.00	99.00	1799.04	1799.04
12.7	98.46	108.85	1789.29	1978.02
12.7	99.24	109.02	1803.31	1981.18

3.2 Hysteretic Curves

The hysteretic curves, which represent the response of the specimens to the displacement control lateral loads, are shown in Figure 8. The BCS-I-1B-33.8 specimen displayed the highest lateral load and the largest hysteretic area.

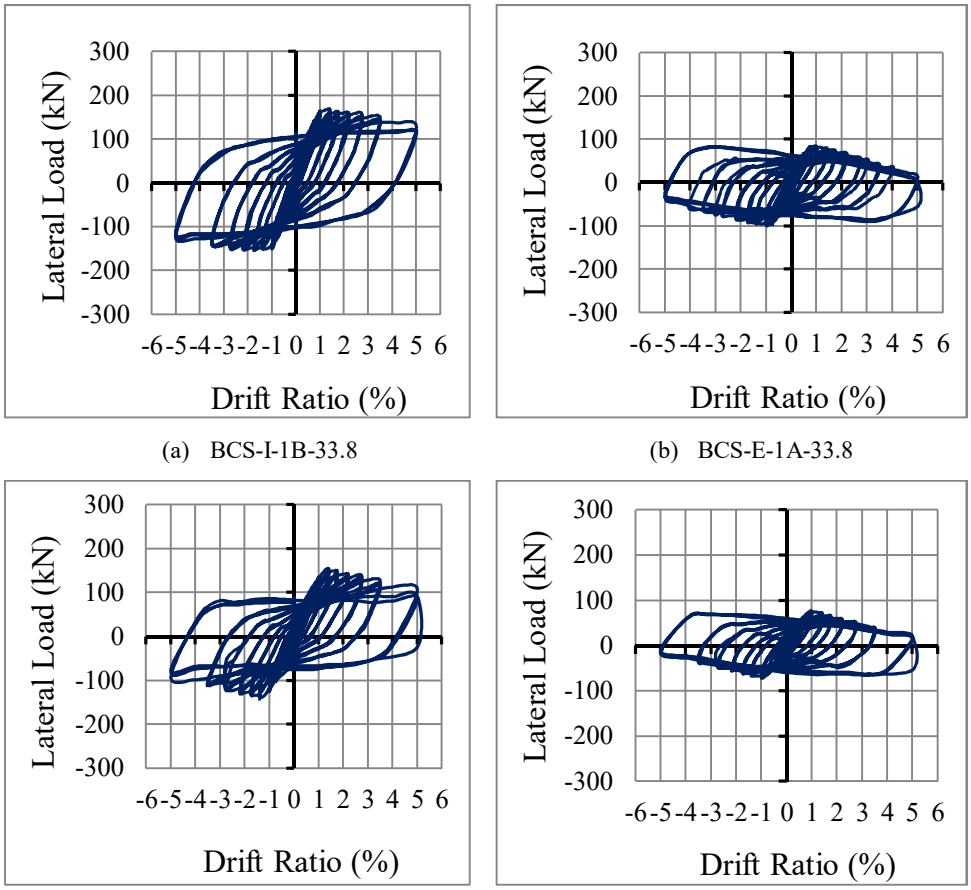

(a) BCS-I-1B-33.8 (b) BCS-E-1A-33.8

(c) BCS-I-2B-22.8 (d) BCS-E-2B-22.8

Figure 8 Hysteretic curves.

3.3 Strain on Plastic Hinges

The value of strain experienced by the mild steel bars and strands were measured using strain gauges. The stress values were determined by the Menegotto-Pinto method [14]. The yield strain in longitudinal mild steel D22 occurred in the plastic hinges and joint zones. Meanwhile, the pre-stressed strands in the plastic hinges and joint zones were still in elastic condition.

In the columns close to joint zones, the vertical longitudinal reinforcements of all specimens were still elastic. The stress-strain curves of longitudinal reinforcement mild steel D22 in the beam plastic hinges are shown in Figure 9.

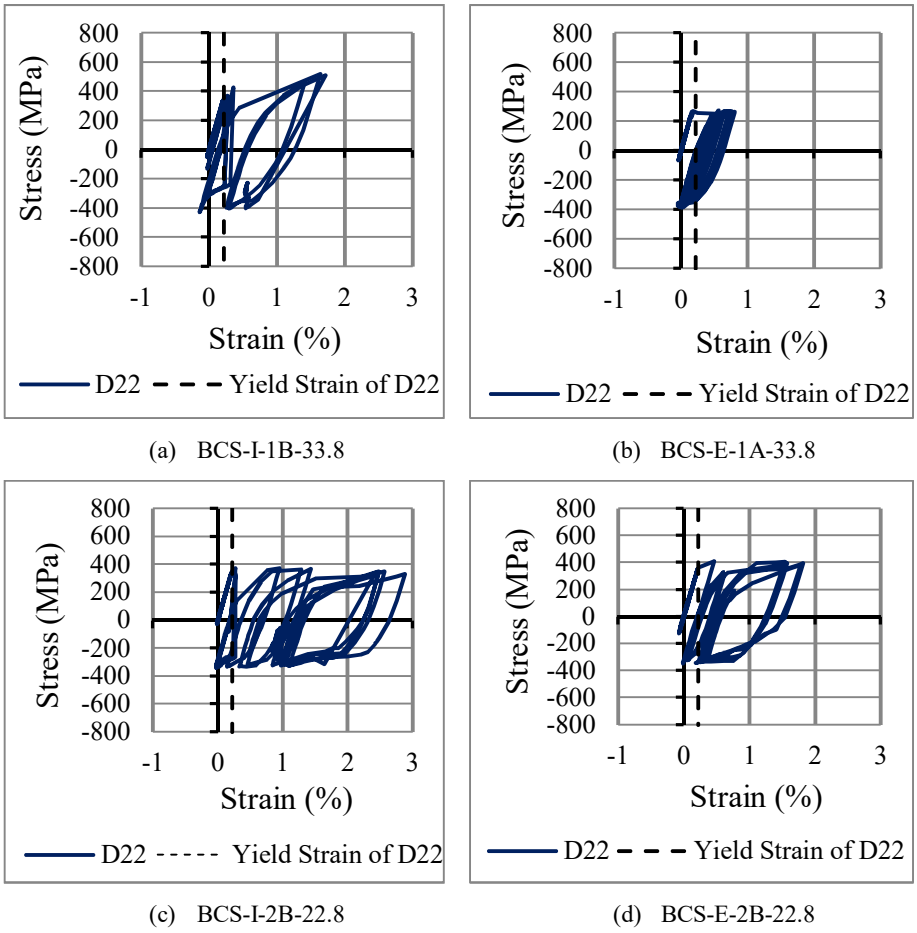

Figure 9 Strain-stress curves.

3.4 Criteria #1 (Strength)

Strength degradation due to large lateral displacement occurs if the specimens achieve their strength limit. A specimen is categorized to have adequate strength if the lateral load for 3.50% drift ratio cycle 3 is equal to or greater than 75% of the peak lateral load [6]. This is suitable for BCS specimens made from NC materials and without pre-stressed reinforcements. In this study, the four specimens were created using RPC and partially pre-stressed reinforcements, and were assessed using criteria approaching actual conditions. The BCS-I-1B-33.8 specimen fulfilled the criteria at 3.50% drift ratio, whilst the other three specimens fulfilled the criteria at lower drift ratios. A summary of strength comparisons of the four specimens is shown in Table 6.

Table 6 Lateral loads and drift ratio at adequate strength.

Specimen	Drift ratio at peak lateral load	Peak lateral load	Maximum drift ratio at adequate strength ratio	Lateral load at adequate strength ratio	Strength ratio ≥ 75%
	(%)	(kN)	(%)	(kN)	(%)
BCS-I-1B-33.8	1.40	+168.10	3.50	+139.00	82.69
BCS-I-1B-33.8	1.75	-153.90	3.50	-135.30	87.91
BCS-E-1A-33.8	1.00	+84.40	2.20	+64.06	75.90
BCS-E-1A-33.8	1.00	-98.30	2.20	-80.10	81.49
BCS-I-2B-22.8	1.40	+154.50	2.75	+127.40	82.46
BCS-I-2B-22.8	1.40	-141.60	2.75	-113.80	80.37
BCS-E-2B-22.8	1.00	+75.70	1.75	+65.80	86.92
BCS-E-2B-22.8	1.00	-71.40	1.75	-60.90	85.29

Note: + push, - pull

3.5 Criteria #2 (Energy Dissipation Ratio)

The relative energy dissipation ratio (β) is the proportion of the area formed by the hysteretic loop (A_h) in relation to the area of a parallelogram formed from the end of the hysteretic loop for 3.50% drift ratio cycle 3 with the slope according to the initial stiffness for 0.2% drift ratio cycle 1 {$(E_1+E_2)(\theta'_1+\theta'_2)$, where E_1 and E_2 are lateral forces and θ_1' and θ_2' are drift ratios on push and pull loading, respectively}. A specimen fulfills the criteria if this ratio is equal to or greater than 0.125. The values of the relative energy dissipation ratio [$\beta=A_h/\{(E_1+E_2)(\theta'_1+\theta'_2)\}$] of all the specimens are shown in Table 7 and the relative energy dissipation increment curves are shown in Figure 10. The results show that all specimens fulfilled the criteria.

Table 7 Relative energy dissipation ratio.

Specimen	Relative Energy Dissipation Ratio at 3.50% *Drift Ratio* Cycle 3	Adequate criteria $\beta \geq 0.125$
BCS-I-1B-33.8	0.585	Yes
BCS-E-1A-33.8	0.880	Yes
BCS-I-2B-22.8	0.633	Yes
BCS-E-2B-22.8	0.664	Yes

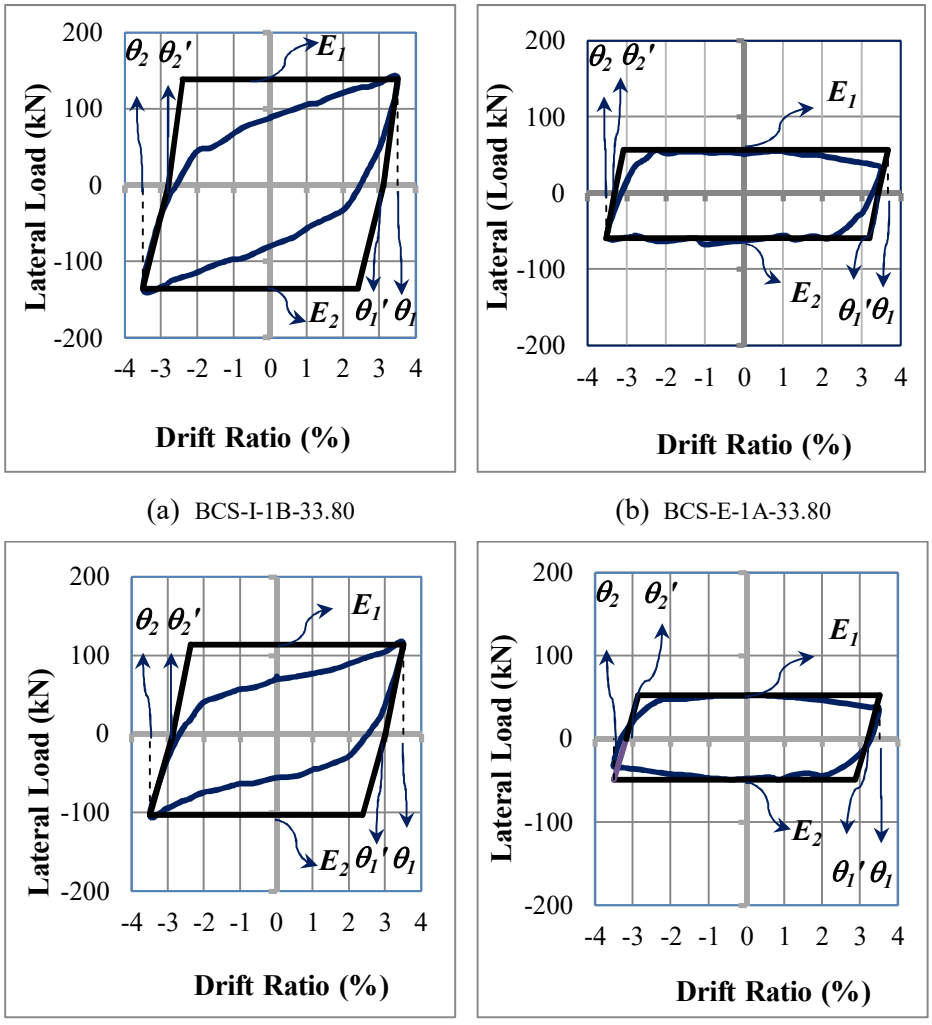

(a) BCS-I-1B-33.80 (b) BCS-E-1A-33.80

(c) BCS-I-2B-22.80 (d) BCS-E-2B-22.80

Figure 10 Relative energy dissipation ratio curves.

3.6 Criteria #3 (Load-Deflection Hysteretic Curve Gradient)

The load-deflection hysteretic curve gradient is the ratio between the gradient limit at -3.50% and +3.50% drift ratios in comparison to the initial gradient (0.2% drift ratio) at the first loading cycle.

A specimen fulfills the third criteria if the gradient ratio is equal to or greater than 0.05. The results show that all specimens had an adequate load-deflection hysteretic curve gradient (Tables 8 and 9).

Table 8 Lateral load-deflection at adequate criteria maximum drift ratio.

Specimen	Deflection	Lateral load	Gradient_1
	δ_1	F_1	$\tan \alpha_1 = F_1/\delta_1$
	(mm)	(kN)	(kN/mm)
	Drift Ratio: 3.50% (push) and 3.50% (pull)		
BCS-I-1B-33.8	+83.64	+139.00	1.66
BCS-I-1B-33.8	-83.73	-135.30	1.62
	Drift Ratio: 2.75% (push) and 3.50% (pull)		
BCS-E-1A-33.8	+61.17	+49.90	0.82
BCS-E-1A-33.8	-77.97	-54.20	0.70
	Drift Ratio: 3.50% (push) and 3.50% (pull)		
BCS-I-2B-22.8	+88.02	+114.10	1.30
BCS-I-2B-22.8	-87.90	-102.60	1.17
	Drift Ratio: 3.50% (push) and 3.50% (pull)		
BCS-E-2B-22.8	+86.55	+36.40	0.42
BCS-E-2B-22.8	-86.34	-33.40	0.39

Note: + push; - pull

Table 9 Lateral load-deflection at drift ratio 0.20% and curve gradient ratios.

Specimen	δ_2	F_2	Gradient_2	Gradient Ratio	Adequate Criteria
	Drift Ratio: 0.20%		$\tan \alpha_2 = F_2/\delta_2$	$\tan \alpha_1/\tan \alpha_2$	>0.05
	(mm)	(kN)	(kN/mm)		
BCS-I-1B-33.8	+4.86	+71.10	14.63	0.11	Yes
BCS-I-1B-33.8	-4.83	-39.30	8.14	0.20	Yes
BCS-E-1A-33.8	+4.14	+42.30	10.22	0.08	Yes
BCS-E-1A-33.8	-4.77	-53.90	11.30	0.06	Yes
BCS-I-2B-22.8	+5.01	+46.30	9.24	0.14	Yes
BCS-I-2B-22.8	-5.25	-33.80	6.42	0.18	Yes
BCS-E-2B-22.7	+4.92	+33.40	6.79	0.06	Yes
BCS-E-2B-22.7	-4.92	-29.70	6.04	0.06	Yes

3.7 Energy Dissipation

Energy dissipation values were determined continuously until the end of loading, i.e. at 5.00% drift ratio. The results showed that the energy dissipation increased along with increasing drift ratio (Figure 11). The cumulative energy dissipation values for each drift ratio and cycle are also shown in Figure 12.

The values of the cumulative dissipation ratio (Table 10) indicate that the specimens with higher PPR values had greater cumulative energy dissipation than their lower PPR counterparts. It can also be seen that each interior BCS

specimen had greater cumulative energy dissipation than the exterior BCS specimens with the same PPR.

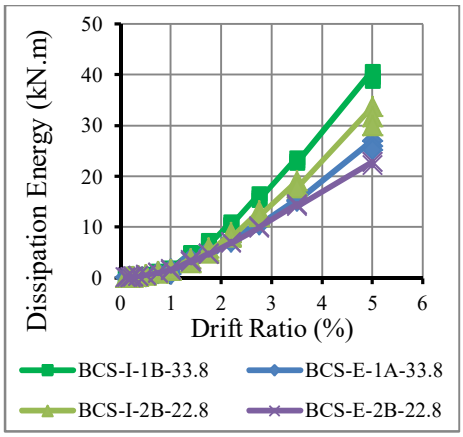

Figure 11 Energy dissipation for each drift ratio and cycle.

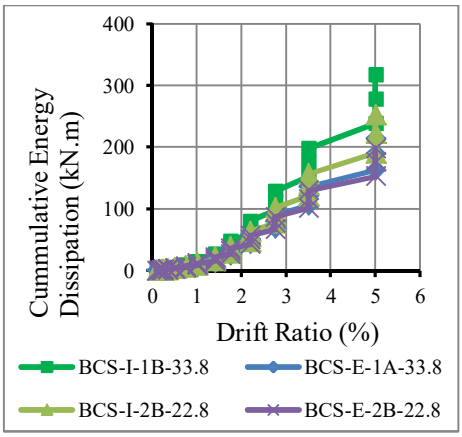

Figure 12 Cumulative energy dissipation for each drift ratio and cycle.

Table 10 Cumulative energy dissipation ratios.

Specimen	Type	Cumulative Energy Dissipation	Ratios_1	Ratios_2
		$E_{d\ Cumulative}$ (kN.m)	$E_d/E_{d\ max.}$	$E_d/E_{d\ min.}$
BCS-I-1B-33.8	Interior	317.81	1.00	1.60
BCS-E-1A-33.8	Exterior	214.73	0.68	1.08
BCS-I-2B-22.8	Interior	252.82	0.80	1.28
BCS-E-2B-22.8	Exterior	198.09	0.62	1.00

3.8 Displacement Ductility

Displacement ductility (μ) was determined as the ratio of the lateral deflection at cycle 3 (δ_3) when the specimens fulfilled all three acceptance criteria for moment frames [6] to the lateral deflection when significant yield (δ_y) occurred. The significant yield points were calculated by the equal area method [15]. They had deflection abscissas and lateral load ordinates as shown in Table 11.

The displacement ductility values (Table 12) show that both interior BCS specimens were more ductile than the exterior BCS specimens with the same PPR. Also, the BCS specimens with a PPR of 33.8% were more ductile than those with a PPR of 22.8%.

Table 11 Significant yield deflection and lateral load.

Specimen	Significant Yield Deflection		Significant Yield Lateral Load	
	δ_y (+)	δ_y (-)	F_y (+)	F_y (-)
	(mm)	(mm)	(kN)	(kN)
BCS-I-1B-33.8	8.10	-8.05	112.20	-91.00
BCS-E-1A-33.8	6.90	-7.95	67.80	-77.10
BCS-I-2B-22.8	8.35	-8.05	89.30	-55.90
BCS-E-2B-22.8	8.20	-8.20	54.20	-48.60

Note: + push; - pull

Table 12 Displacement ductility.

Specimen	Drift Ratio (+/-)	Lateral Deflect-ion (+)	Lateral Deflect-ion (-)	Ducti-lity (+)	Ducti-lity (-)	μ/μ_{min} (+)	μ/μ_{min} (-)
		δ_3	δ_3	μ	μ		
	(%)	(mm)	(mm)				
BCS-I-1B-33.8	3.50	83.64	-83.73	10.33	10.40	1.96	1.97
BCS-E-1A-33.8	2.20	47.97	-48.96	6.95	6.16	1.32	1.17
BCS-I-2B-22.8	2.75	68.88	-69.45	8.25	8.63	1.56	1.64
BCS-E-2B-22.8	1.75	43.29	-43.23	5.28	5.27	1.00	1.00

3.9 Seismic Performance Level

The previous analyses of the strength, energy dissipation ratio, and load-deflection hysteretic curve gradient of the specimens show that three specimens had a seismic performance level of Collapse Prevention (CP), because they satisfied the three acceptance criteria for moment frames at lateral drift ratios ranging from 2.0% to 4.0%, and one specimen had a seismic performance level of Life Safety (LS), because it satisfied the three acceptance criteria for moment frames at lateral drift ratios ranging between 1.0% to 2.0% (Table 13).

In addition to performance levels based on lateral drift ratios, the specimens' performance was also assessed based on the plastic rotation angle. The ratio of ultimate shear to nominal shear (V_u/V_n) can be expressed as the ratio of ultimate moment to nominal moment (M_u/M_n), where M_u is the ultimate moment when the specimen fulfills the acceptance criteria for moment frames and M_n is the nominal moment based on the material test results (Tables 3, 4, and 5) and details of the specimens (Figures 1 to 4).

Table 13 Performance Level Based on Lateral Drift Ratio.

Specimen	Drift Ratio	Performance Level
BCS-I-1B-33.8	3.50%	Collapse Prevention
BCS-E-1A-33.8	2.20%	Collapse Prevention
BCS-I-2B-22.8	2.75%	Collapse Prevention
BCS-E-2B-22.8	1.75%	Life Safety

The ultimate moment (M_u), yield moment (M_y), maximum moment (M_a), and crack moment (M_{cr}) are the moments in the intersections between beams and columns when ultimate load (F_u), yield load (F_y), maximum load (F_a), and crack load (F_{cr}) occur. The nominal moment (M_n) values of the specimens with a PPR of 33.8% and 22.8% are 149.68 and 134.56 kN.m, respectively. The plastic hinge length (l_p) was 300 mm.

The plastic rotation is expressed in the following Eq. (1):

$$\theta_p = \theta_u - \theta_y \tag{1}$$

where:

θ_p : plastic rotation (radians)
θ_u : ultimate rotation (radians)
θ_y : yield rotation (radians)

The ultimate rotation is expressed in the following Eq. (2):

$$\theta_u = \left(\frac{M_u}{E_c I_e}\right) l_p \tag{2}$$

where E_c is the elastic modulus in MPa.

The yield rotation is expressed in the following Eq.(3):

$$\theta_y = \left(\frac{M_y}{E_c I_e}\right) l_p \tag{3}$$

The effective moment of inertia (I_e) is expressed in the following Eq.(4):

$$I_e = \left(\frac{M_{cr}}{M_a}\right)^3 I_g + \left[1 - \left(\frac{M_{cr}}{M_a}\right)^3\right] I_{cr} \leq I_g \tag{4}$$

The crack moment of inertia (I_{cr}) and the gross moment of inertia (I_g) were determined based on beam section data of each specimen (Figures 1 to 4). Tables 14 to 16 show the values of the average crack moment, maximum loads, average maximum moment, and the effective inertia moment for all four specimens.

Table 14 Crack moment.

Specimen	Push Crack Load	Pull Crack Load	Average Crack Moment
	F_{cr} (+)	F_{cr} (-)	$M_{cr\ average}$
	(kN)	(kN)	(kN.m)
BCS-I-1B-33.8	48.90	-29.40	50.76
BCS-E-1A-33.8	34.40	-53.90	79.73
BCS-I-2B-22.8	38.30	-26.10	43.36
BCS-E-2B-22.8	24.80	-29.70	53.94

Table 15 Maximum load.

Specimen	Drift Ratio	Push Max. Load	Drift Ratio	Pull Max. Load
	F_a (+)		F_a (-)	
	(%)	(kN)	(%)	(kN)
BCS-I-1B-33.8	1.41	168.10	1.75	-153.90
BCS-E-1A-33.8	1.00	84.40	1.00	-98.30
BCS-I-2B-22.8	1.41	154.50	1.41	-141.60
BCS-E-2B-22.8	1.00	75.70	1.00	-71.40

Table 16 Average maximum moment and effective inertia moment.

Specimen	Average Maximum Moment	Effective Inertia Moment
	$M_{a\ average}$	I_e
	(kN.m)	(m^4)
BCS-I-1B-33.8	128.49	4.18E-04
BCS-E-1A-33.8	237.42	2.32E-04
BCS-I-2B-22.8	125.01	3.99E-04
BCS-E-2B-22.8	200.13	3.04E-04

Table 17 Yield rotation.

Specimen	Yield Load (+)	Yield Load (-)	Average Yield Moment	Yield Rotation
	F_y (+)	F_y (-)	$M_{y\ average}$	θ_y
	(kN)	(kN)	(kN.m)	(rad)
BCS-I-1B-33.8	112.20	-91.00	81.08	1.43E-03
BCS-E-1A-33.8	67.80	-77.10	188.30	6.00E-03
BCS-I-2B-22.8	89.30	-55.90	61.30	1.13E-03
BCS-E-2B-22.8	54.20	-48.60	139.86	3.39E-03

By using Eqs. (1) to (4), the values of yield rotation and ultimate rotation were determined (Tables 17 and 18). Based on the values of plastic rotation, value category of $P/(A_g f_c') \leq 0.1$, and $V_u/V_n \leq 1.5$ [7] (where P is the axial constant load on the top of the specimen columns), the specimens had moment ratio values and seismic performance levels of Collapse Prevention (Tables 19 and 20, respectively), which indicates that the specimens were still stable until being partially or fully damaged due to the seismic loads.

Table 18 Ultimate rotation.

Specimen	Ultimate Load (+)	Ultimate Load (-)	Average Plastic Moment	Ultimate Rotation
	F_u	F_u	$M_{u\ average}$	θ_u
	(kN)	(kN)	(kN.m)	(rad)
BCS-I-1B-33.8	148.20	-141.60	115.64	2.04E-03
BCS-E-1A-33.8	67.10	-83.00	195.06	6.22E-03
BCS-I-2B-22.8	127.4	-113.8	101.83	1.88E-03
BCS-E-2B-22.8	62.2	-60.9	167.48	4.06E-03

Table 19 Moment ratio.

Specimen	Constant Axial Load Ratio	Nominal Moment	Moment Ratio
	$P/(A_g f_c') \leq 0,1$	M_n	$M_u/M_n \leq 1.5$
		(kN.m)	
BCS-I-1B-33.8	0.10	149.68	0.77
BCS-E-1A-33.8	0.10	149.68	1.30
BCS-I-2B-22.8	0.10	134.56	0.75
BCS-E-2B-22.8	0.10	134.56	1.24

Table 20 Plastic Rotation and Structure Performance Level

Specimen	Plastic Rotation	Structure Performance Level
	$\theta_p = \theta_u - \theta_y$	
	(radians)	
BCS-I-1B-33.8	6.10E-04	Collapse Prevention
BCS-E-1A-33.8	2.15E-04	Collapse Prevention
BCS-I-2B-22.8	7.50E-04	Collapse Prevention
BCS-E-2B-22.8	6.70E-04	Collapse Prevention

4 Conclusions

The BCS-I-1B-33.8 specimen with a PPR of 33.8% had the highest strength due to a higher nominal moment of the partially pre-stressed reinforcement, which

improved the ability to resist moment. The nominal moment influenced behavior where all specimens with a PPR of 33.8% had greater ductility and energy dissipation than the specimens with a PPR of 22.8%. Thus, PPR values above the maximum limit of 25% [1,2] increased the ductility and energy dissipation of the reactive powder concrete specimens.

The two plastic hinges on the interior specimens provided higher strength to resist lateral loads and the ability to dissipate energy more than the exterior specimens with the same PPR.

Three specimens, BCS-I-1B-33.8, BCS-E-1A-33.8, and BCS-I-2B-22.8, had a seismic performance level of Collapse Prevention (CP) based on the acceptance criteria for moment frames [6,7]. Specimens with a PPR of 33.8% and two plastic hinges (interior BCS) had the ability to resist higher lateral loads and were more capable of maintaining stiffness on greater drift ratios than specimens with only one plastic hinge (exterior BCS) and a PPR of 22.8%.

Based on the drift ratios, three specimens achieved a Collapse Prevention seismic performance level due to a higher nominal moment and the number of plastic hinges, while one specimen achieved a Life Safety seismic performance level. Based on the plastic rotation, all four specimens achieved a Collapse Prevention seismic performance level, which indicates that the specimens were still stable until partial or full damage conditions due to the seismic loads.

5 Recommendations

To improve the performance of exterior beam-column sub-assemblage specimens, the addition of longitudinal (mild steel bars or pre-stressed strands) and transversal reinforcements in beam plastic hinges is required. The additional reinforcements will also reduce crack widths and provide higher energy dissipation, as well as significantly reducing strength and stiffness degradation. When designing the additional longitudinal pre-stressed strands, the ductility performance of the external beam-column sub-assemblage should be taken into consideration.

Acknowledgements

The primary financial support for this research program was provided by P.T. Wijaya Karya Beton, Indonesia, under joint research with the Faculty of Civil and Environment Engineering, Institut Teknologi Bandung under contract no. KU.09.09/OA.WB.191/2014 and 167/I1.C09/DN/2014.

References

[1] BSN, SNI 03–2847–2013 *The Design Method of Concrete Structure for Buildings*, Jakarta, 2013. (Text in Indonesian)

[2] ACI Committee, *Building Code Requirements for Structural Concrete* (ACI 318-14) and Commentary, ACI, Farmington Hills, United States, 2014.

[3] Richard, P. & Cheyrezy, M., *RPC with High Ductility and 200-800 MPa Compression Strength*, Proceeding of V. Mohan Malhotra Symposium, pp. 507-518, Farmington Hills, 1994.

[4] Richard, P. & Cheyrezy, M., *Composition of Reactive Powder Concrete,* Cement and Concrete Research, **25** (7), pp. 1501-1511, 1995.

[5] Patel, P.A., Desai, A.K. & Desai, J.A., *Evaluation of Engineering Properties for Polypropylene Fiber Reinforced Concrete*, International Journal of Advanced Engineering Technology, **3**(1), pp. 42-45, 2012.

[6] ACI Committee, *Acceptance Criteria for Moment Frames Based on Structural Testing and Commentary*, ACI 374.1-05, Farmington Hills, United States, 2005.

[7] ACI Committee, *Guide for Testing RC Structural Elements under Slowly Applied Simulated Seismic Loads*, ACI 374.2R-13, Farmington Hills, United States, 2013.

[8] Nurjannah, S.A., Budiono, B., Imran, I. & Sugiri, S., *Performance of RPC Partial Pre-stressed BC Sub-assemblage Structure System with PPR Exceeds 30%,* 3rd International Conference on Rehabilitation and Maintenance in Civil Engineering, Solo, Indonesia, pp. 126-131, 2015.

[9] Nurjannah, S.A., Budiono, B., Imran, I. & Sugiri, S., *Hysteretic Behavior of Reactive Powder Concrete Partially Pre-stressed Interior Beam-Column Sub-assemblages in Finite Element Modeling,* Jurnal Teknik Sipil ITB, **22** (3) pp. 175-190, 2015. (Text in Indonesian)

[10] Gowripalan, N., Watters, R., Gilbert, R.I. & Cavill, B., *RPC for Precast Structural Concrete-Research and Dev,* in 21st Biennial Conf. of The Concrete Institute of Australia, Brisbane, Australia, pp. 99-108, 2003.

[11] Menefy, L., *Investigation of RPC and Its Damping Characteristics When Utilized in Beam Elements*, Thesis of Doctor Philosophy, School of Engineering, Griffith University, Gold Coast, Australia, 2007.

[12] Naibaho, P.R., Budiono, B., Surono, A. & Pane, I., *Experimental Study of Exterior Beam-Column Connection Using Reactive Powder Concrete under Cyclic Load,* Proc. National Conference of Post Graduate of Civil Engineering, Bandung, Indonesia, pp. 85-95, 2013. (Text in Indonesian)

[13] ASTM, ASTM A416/A416 M., *Standard Specification for Steel Strand, Uncoated Seven-Wire for Pre-stressed Concrete*, Washington D.C., United States, 2006.

[14] Menegotto, M. & Pinto, P.E., *Method of Analysis for Cyclically Loaded Reinforced Concrete Plane Frames*, Proceeding International Association for Bridge and Structural Engineering Symposium, Lisbon, Portugal, **13** pp. 15-22, 1973.
[15] American Society of Civil Engineers, *FEMA 356: Prestandard and Commentary for the Seismic Rehabilitation of Buildings*, Virginia, United States, 2000.